International Journal of Minerals, Metallurgy and Materials
Volume 21, Number 3, March 2014, Page 266
DOI: 10.1007/s12613-014-0904-y

Mechanical properties and characteristics of nanometer-sized precipitates in hot-rolled low-carbon ferritic steel

Xiao-pei Wang, Ai-min Zhao, Zheng-zhi Zhao, Yao Huang, Liang Li, and Qing He

Engineering Research Institute, University of Science and Technology Beijing, Beijing 100083, China
(Received: 29 July 2013; revised: 21 November 2013; accepted: 22 November 2013)

Abstract: The microstructures and properties of hot-rolled low-carbon ferritic steel have been investigated by optical microscopy, field-emission scanning electron microscopy, transmission electron microscopy, and tensile tests after isothermal transformation from 600°C to 700°C for 60 min. It is found that the strength of the steel decreases with the increment of isothermal temperature, whereas the hole expansion ratio and the fraction of high-angle grain boundaries increase. A large amount of nanometer-sized carbides were homogeneously distributed throughout the material, and fine (Ti, Mo)C precipitates have a significant precipitation strengthening effect on the ferrite phase because of their high density. The nanometer-sized carbides have a lattice parameter of 0.411–0.431 nm. After isothermal transformation at 650°C for 60 min, the ferrite phase can be strengthened above 300 MPa by precipitation strengthening according to the Ashby-Orowan mechanism.

Keywords: ferritic steel; nanoparticles; mechanical properties; carbides; precipitation; strengthening

1. Introduction

It is well established that the addition of a small amount of micro-alloying elements such as niobium (Nb), vanadium (V), and titanium (Ti) into steel plays significant roles in improving its properties [1–3]. The precipitation behavior of these micro-alloying elements and their strengthening mechanisms have been investigated by many researchers [4–7]. High-strength low-alloy (HSLA) steels usually possess yield strengths of about 400–500 MPa, and the contribution of precipitation hardening to these values was considered to be minor, since many of the alloying elements were added to HSLA steels in the past basically for the strengthening of grain refinement [7]. However, in a recent study conducted at JFE steel [8], tensile strengths of up to 780 MPa have been achieved in Ti–Mo-bearing hot-rolled sheet steels by producing microstructures that consist of a ferritic matrix with nanometer-sized carbides. Precipitation strengthening due to nanometer-sized carbides in these ferrite steels has been estimated to be approximately 300 MPa, which is 2–3 times higher than that of conventional precipitation hardening in micro-alloyed steels. This value draws significant attention, and studies on nanometer-sized Ti–Mo complex carbides formed in the ferrite matrix have been reported by many researchers [9–10]. This study investigates the effect of isothermal temperature on the microstructures and properties of ferrite steel and studies the characteristics of nanometer-sized carbides precipitated in the ferrite matrix. The amount of precipitation hardening by the fine precipitates is also estimated on the basis of the Ashby-Orowan mechanism.

2. Experimental

Experimental hot-rolled ferritic steel was prepared in a 50-kg vacuum induction furnace and casted into ingots in dimensions of 60 mm × 60 mm × 60 mm (thickness × width × length). The basic composition of the investigated steel is Fe–0.043C–1.57Mn–0.088Si–0.10Ti–0.26Mo–0.007P–0.003S–0.005N (wt%), which was designed to obtain a tensile strength of around 780 MPa and a microstructure consisting of a ferrite matrix strengthened by finely precipitated carbides.

Fig. 1 shows the scheme of the hot-rolling process. The ingots were reheated at 1250°C for 90 min for solution

Corresponding author: Ai-min Zhao E-mail: aimin.zhao@ustb.edu.cn

treatment and subsequently hot-rolled at a finishing temperature of approximately 900°C according to a thickness change of 60 mm → 42 mm → 29 mm → 20 mm → 12 mm → 6 mm → 3.2 mm. After hot rolling, the rolled plates were immediately cooled down to 600°C, 650°C, or 700°C at a cooling rate of 30°C/s and maintained at that temperature for 60 min before air cooling to room temperature.

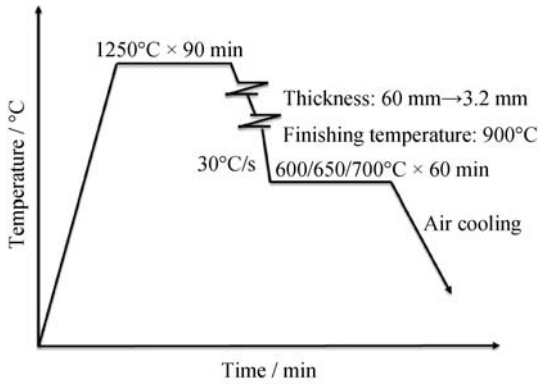

Fig. 1. Schematic diagram of the hot-rolling process.

The mechanical properties of steel were tested according to the Chinese National Standard GB/T 228.1–2010. The microstructure was characterized by optical microscopy (OM) and field-emission scanning electron microscopy (FE-SEM). Electron back-scattered diffraction (EBSD) measurements were performed using FE-SEM to investigate the orientations of grains, and the grain size of ferrite was measured by Image-Pro Plus software.

The hole expansion test was performed in a hydraulic sheet ductility tester according to the Chinese National Standard GB/T 15825.4–2008. A hole of 10 mm in diameter is punched out and then stretched by a conic punch with the top angle of 60°. When a crack through the thickness is generated, the diameter of the expanded hole d (mm) is measured. The hole expansion ratio λ as an index of stretch flange formability is calculated by the following equation:

$$\lambda = \frac{d-10}{10} \times 100\% \quad (1)$$

Transmission electron microscopy (TEM) specimens were prepared from 0.30-mm-thick discs sliced from a mechanics performance testing specimen. The disc was thinned to 0.05 mm by abrasion on SiC paper and then twin-jet electropolished to perforation using a mixture of 5vol% perchloric acid, 5vol% glycerol, and 90vol% ethanol at 20–30°C by applying a potential of 35 V. The characteristics of the precipitated particles were examined using a field-emission-gun transmission electron microscope (FEG- TEM; JEM-2010) operated at 200 kV.

3. Results and discussion

3.1. Microstructure and mechanical properties

Fig. 2 shows the OM and SEM images of the experimental steel at an isothermal holding temperature of 600°C for 60 min. The matrix microstructure of the steel was polygonal ferrite, while pearlite and large cementite were not observed.

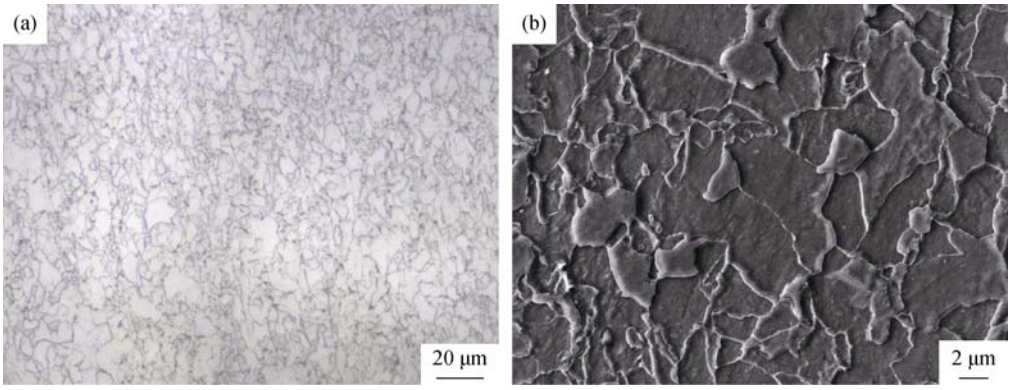

Fig. 2. Images of the steel isothermally treated at 600°C: (a) OM and (b) SEM.

The yield strength (YS), ultimate tensile strength (UTS), elongation, and average ferrite grain size of the experimental steel at different isothermal temperatures are schematized in Table 1. With the decrease of the isothermal temperature, the yield strength and tensile strength of the steel increase, but the elongation and average ferrite size of the steel decrease.

Table 1. Mechanical properties and average grain size at different isothermal temperatures

T / °C	YS / MPa	UTS / MPa	Elongation / %	Grain size / μm
700	590	635	22.4	7.8
650	655	710	20.9	7.2
600	735	780	20.0	6.5

As the nucleation rate of ferrite increases at a lower isothermal temperature, the ferrite grain size decreases [9]. This will enlarge the strength contributed by grain-refinement strengthening. In addition, carbides precipitated during the γ → α isothermal transformation become finer and denser at a lower isothermal temperature [8–9] and the strength due to precipitation strengthening will be larger according to the Ashby-Orowan relationships [11]. The effects above result in an increment in strength at a higher isothermal temperature. The elongation is relatively insensitive to the transformation temperature. The fraction and intensity of the precipitated particles are greater and the ductility is worse [12].

After isothermal transformation at 600°C for 60 min, the tensile strength of the experimental steel can successfully achieve 780 MPa with an elongation of 20% mainly because of the precipitation strengthening of nanometer-sized carbides, which will be discussed later.

3.2. EBSD analysis

The orientation imaging maps and grain misorientation angle distributions from EBSD are presented in Fig. 3. The fraction of high-angle grain boundaries increases with increasing isothermal temperature. The fraction of grain misorientation angles higher than 15° is as high as 84% after isothermal transformation at 700°C for 60 min, which is 77% at 650°C and 70% at 600°C, respectively.

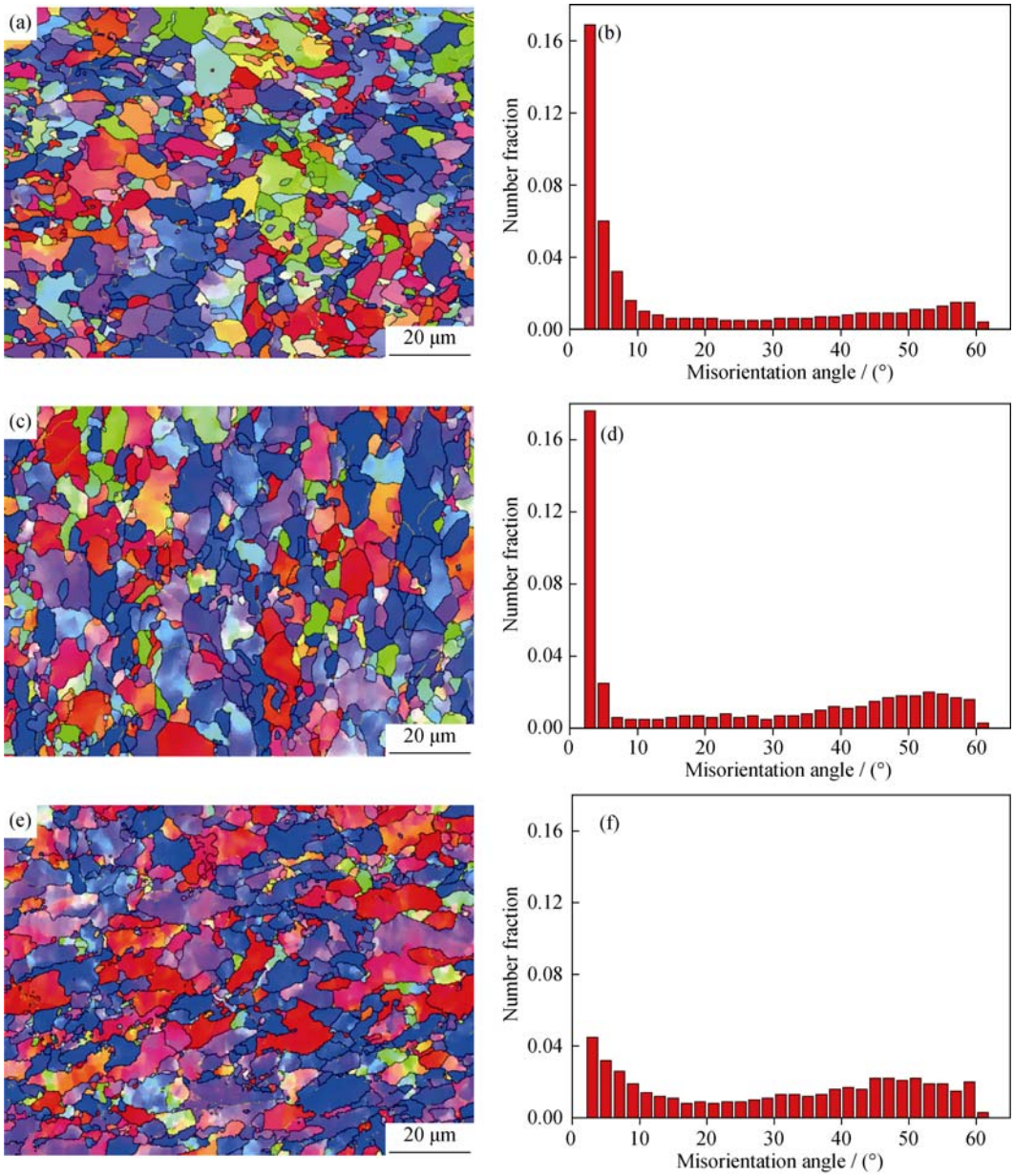

Fig. 3. EBSD orientation imaging maps and misorientation angle distributions at (a, b) 600°C, (c, d) 650°C, and (e, f) 700°C.

The high-angle grain boundary can effectively inhibit crack propagation and improve the toughness of the steel, whereas the low-angle grain boundary has no significant effects [13–14], which results in an increment of the hole expansion ratio at a higher isothermal temperature as it will be discussed later.

3.3. Hole expansion test

Fig. 4 shows the hole expansion ratio of the steel isothermally treated at different temperatures. The hole expansion ratio, which is an index of stretch flange formability, decreases with the reduction in isothermal temperature. The hole expansion ratio is 90% and 111% at 600°C and 700°C, respectively. There is a sharp rise in the hole expansion ratio when the isothermal temperature changes from 600°C to 650°C, whereas no significant increment is made when the isothermal temperature varies from 650°C to 700°C.

As can be seen from Fig. 3, the microstructure of the steel is more heterogeneous at a lower isothermal temperature. It is well known that microstructure heterogeneity is detrimental to the hole expansion ratio [15–16]. High microstructural homogeneity gives a greater resistance to void initiation and propagation during punching and the subsequent expanding operation [15]. In addition, the fraction of high angle grain boundaries, which can effectively inhibit the propagation of cracks and improve the toughness of the steel, increases at a higher isothermal temperature. Thus, the stretch flange formability will be better at a higher isothermal temperature.

The SEM images of the punched surface layer isothermally treated at 700°C for 60 min are displayed in Fig. 5. Numerous microvoids or microcracks are observed, whose positions are generally with their long axes parallel to the punching direction. There are also many large inclusions of approximately 3 μm in diameter in the pierced surface (Fig. 5(c)). The microvoids, microcracks, and inclusions are the crack source, which lead to failure in the hole expansion test.

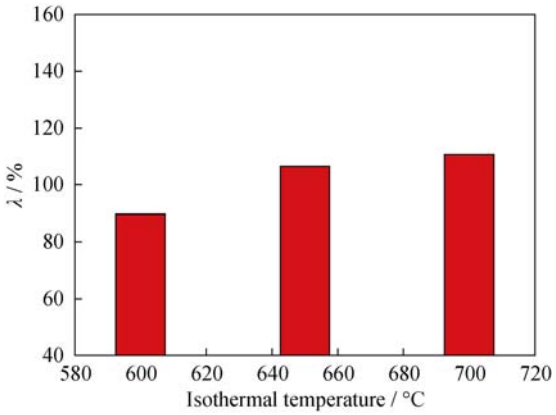

Fig. 4. Hole expansion ratio λ at different isothermal temperatures.

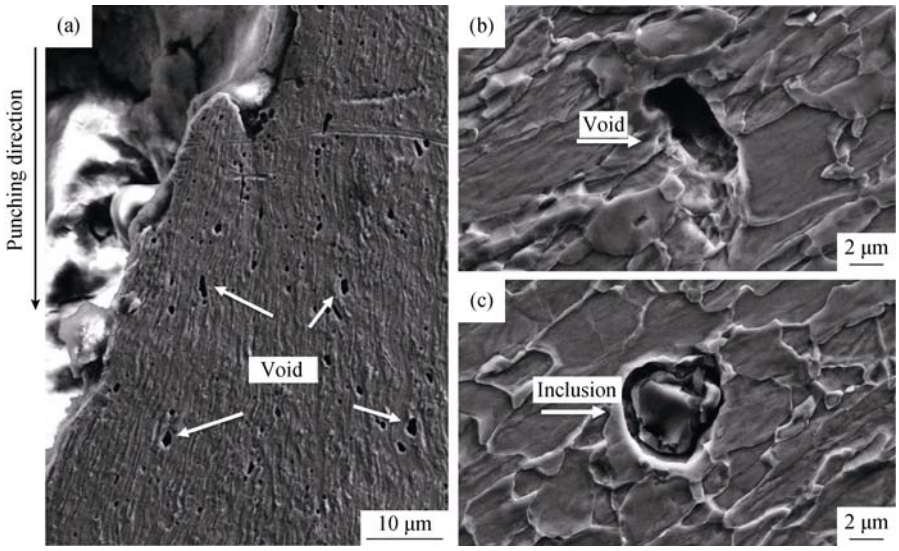

Fig. 5. SEM images of the punched surface layer isothermally treated at 700°C: (a) punched surface layer, (b) a microvoid and (c) an inclusion.

3.4. TEM observation

The precipitated carbides in the ferrite matrix isothermally treated at 650°C for 60 min can be clearly identified by TEM (Fig. 6). A large amount of nanometer-sized carbides are observed and the finely dispersed precipitates are homogeneously distributed throughout the material. By using duplicate energy-dispersive X-ray spectroscopy (EDXS) analysis, these nanometer-sized particles are determined to be (Ti, Mo)C carbides with a NaCl-type crystal structure, and they have a significant precipitation strengthening effect on the ferrite phase due to their high density [8, 17].

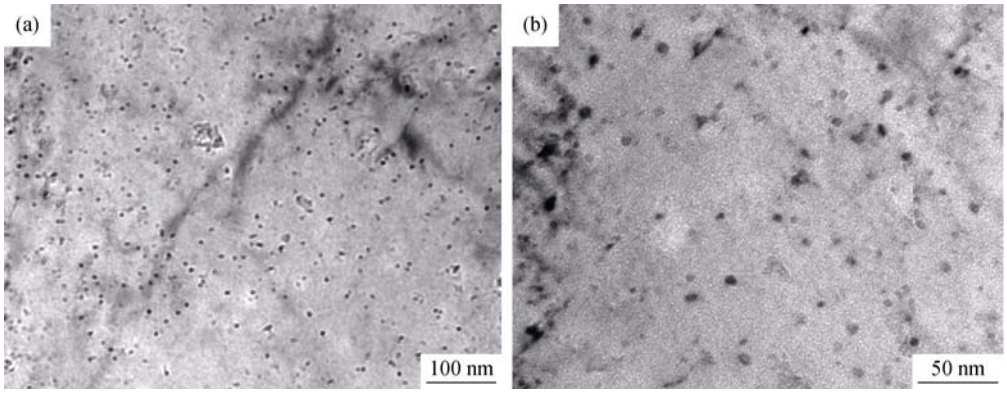

Fig. 6. TEM micrographs of nanometer-sized carbides in the steel at 650°C.

Fig. 7 shows the interphase precipitation of (Ti, Mo)C carbides, which nucleated densely on the austenite/ferrite interface during the transformation from austenite to ferrite. The characteristics of the interphase-precipitated carbides have been reported extensively in recent years [9–10, 17–18]. There are two different types of interphase precipitation carbides, i.e., planar interphase precipitation and curved interphase precipitation [17, 19]. The planar interphase precipitates grow according to the ledge mechanism. This mechanism assumes that precipitation occurs on planar, low energy, semicoherent, immobile interfaces formed by the passage of a high energy ledge, which moves too fast to act as a nucleation site [20]. The quasiledge mechanism was proposed for precipitation on high energy, disordered, austenite-ferrite interphase boundaries that have been immobilized by copious precipitation, forming curved sheets of precipitates [21]. The row-like characteristic is the prominent feature of interphase precipitation, and the row spacing becomes larger with increments in isothermal temperature [9, 18].

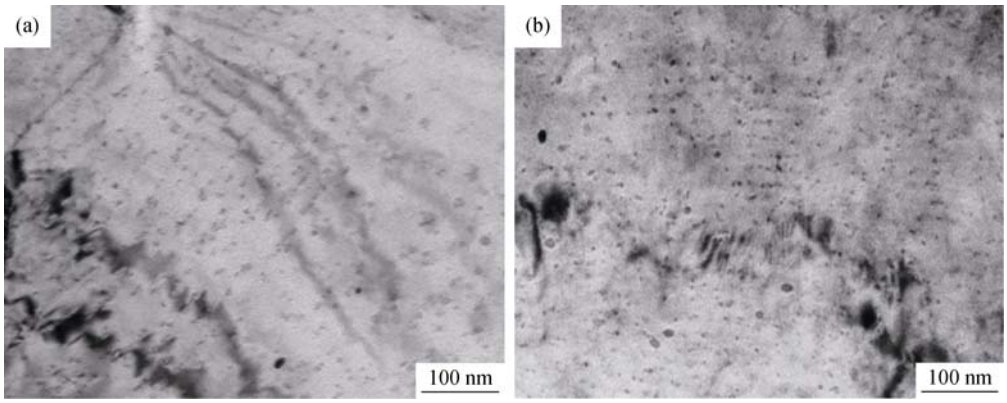

Fig. 7. Planar interphase precipitation (a) and curved interphase precipitation (b) of (Ti, Mo)C at 650°C.

3.5. High resolution TEM observation

A high-resolution TEM (HRTEM) investigation of the nanometer-sized carbides was performed, and an example of a lattice image of the (Ti, Mo)C carbide isothermally treated at 650°C for 60 min is presented in Fig. 8. The size of the carbide is 5.24 nm in length and 4.75 nm in width, and a diameter of 5.63 nm can be obtained by converting the area of the rectangle into a circle. The average diameter of the nanometer- sized carbides is 5.12 nm, which results from 20 carbides.

The corresponding selected area diffraction patterns (SADP) in Fig. 8(b) reveal that the (Ti, Mo)C carbide exhibits a B-N orientation ($(100)_{MC}||(100)_{ferrite}$ and $[011]_{MC}||[001]_{ferrite}$) with respect to the ferrite matrix, which was also observed by Honeycombe and Mehl [22] in vanadium steels. The HRTEM observation in Fig. 8(a) is along the zone axis $[011]_{(Ti, Mo)C}||[001]_{ferrite}$. Under this condition, the corresponding SADP indicates there is interaction between $(200)_{(Ti, Mo)C}$ and $(200)_{ferrite}$. According to the analyses of Hung *et al.* [23], the spacing for producing Moiré fringes can be presented as

$$L = d_{200\text{ferrite}} \times d_{200(\text{Ti, Mo})\text{C}} / | d_{200\text{ferrite}} - d_{200(\text{Ti, Mo})\text{C}} | \quad (2)$$

where L is the spacing of Moiré fringes, $d_{200\text{ferrite}}$ and $d_{200(\text{Ti, Mo})\text{C}}$ are the interplanar spacings of $(200)_{ferrite}$ and $(200)_{(Ti, Mo)C}$, respectively. Given the measured spacing of Moiré fringes (0.430–0.474 nm) and the lattice parameter of ferrite (0.287 nm), the lattice parameter of (Ti, Mo)C can be determined by Eq. (2) to be 0.411–0.431 nm.

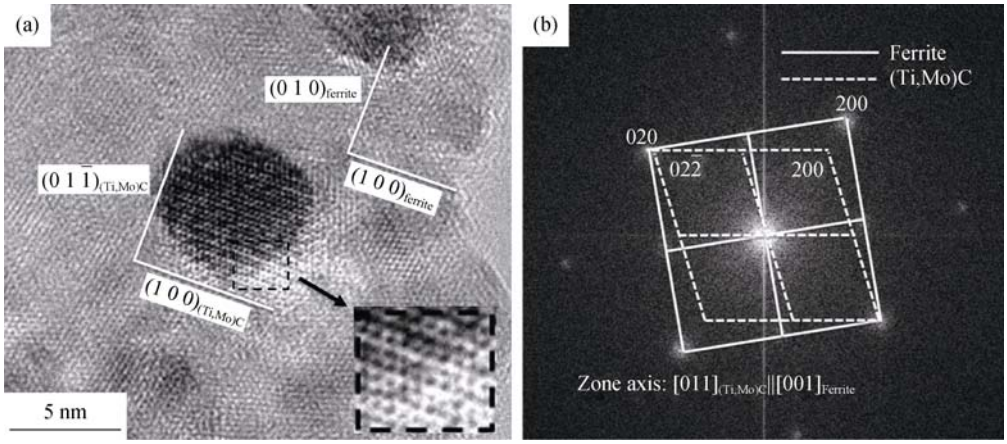

Fig. 8. (a) High resolution transmission electron microscopy (HRTEM) image of (Ti, Mo)C carbide and (b) the corresponding selected area diffraction patterns for the steel isothermally treated at 650°C.

3.6. Precipitation strengthening

The Ashby-Orowan mechanism is well known as a relationship between the diameter of precipitates and amount of precipitation strengthening. The increased yield strength contributed by precipitation strengthening of the nanometer-sized carbides can be estimated by [11]

$$\Delta\sigma_{\mathrm{Pre}} = (0.538Gbf^{1/2}/X)\ln(X/2b) \quad (3)$$

where $\Delta\sigma_{\mathrm{Pre}}$ is the increase in yield strength due to precipitation strengthening, G is the shear modulus (81600 MPa), b is the Burgers vector (0.248 nm) [11], f is the volume fraction of the precipitated carbides, and X is the average diameter of the precipitates. It is assumed that all of the carbon in the steel forms the nanometer-sized carbides because no cementite was generated. Yamada *et al.* [17] reported that the typical composition of (Ti, Mo)C is $(Ti_{0.54}Mo_{0.46})C$, which is consistent with Funakawa's findings [8]. Thus, the volume fraction of the nanometer-sized carbides can be estimated as f = 0.44% with the (Ti, Mo)C lattice parameter of 0.411 nm and carbon content in steel of 0.047%. The strength contributed by precipitation strengthening calculated by Eq. (3) is 329 MPa when the average diameter of the nanometer-sized carbides is 5.12 nm, which indicates that the ferrite phase can be strengthened above 300 MPa by precipitation strengthening in the steel isothermally treated at 650°C for 60 min.

4. Conclusions

Hot-rolled low-carbon ferritic steel isothermally treated at 600°C for 60 min can achieve a 780 MPa tensile strength with an elongation of 20.0% and a hole expansion ratio of 90%. The strength of the steel enhances with the reduction of isothermal temperature, because the grain-refinement strengthening and precipitation strengthening increase at lower isothermal temperature. As the isothermal temperature increases, the hole expansion ratio becomes larger due to the higher microstructural homogeneity and the increase of the fraction of high-angle grain boundaries at a higher isothermal temperature. The nanometer-sized carbides have a lattice parameter of 0.411–0.431 nm. After isothermal transformation at 650°C for 60 min, the ferrite phase can be strengthened above 300 MPa by precipitation strengthening in the steel.

Acknowledgements

The authors are grateful for the financial support by the National Natural Science Foundation of China (No. 51271035) and the Specialized Research Fund for the Doctoral Program of Higher Education of China (No. 20110006110007).

References

[1] Y.F. Shen, C.M. Wang, and X. Sun, A micro-alloyed ferritic steel strengthened by nanoscale precipitates, *Mater. Sci. Eng. A*, 528(2011), No. 28, p. 8150.

[2] Z.G. Wang, A.M. Zhao, Z.Z. Zhao, J.Y. Chen, D. Tang, and G.S. Zhu, Microstructures and mechanical properties of C–Mn–Cr–Nb and C–Mn–Si–Nb ultra-high strength dual-phase steels, *Int. J. Miner. Metall. Mater.*, 19(2012), No. 10, p. 915.

[3] B.K. Show, R. Veerababu, R. Balamuralikrishnan, and G. Malakondaiah, Effect of vanadium and titanium modification on the microstructure and mechanical properties of a micro-alloyed HSLA steel, *Mater. Sci. Eng. A*, 527(2010), No. 6, p. 1595.

[4] R. Lagneborg and S. Zajac, A model for interphase precipitation in V-microalloyed structural steels, *Metall. Mater. Trans. A*, 32(2001), No. 1, p. 39.

[5] Y.Z. Zhu and J.P. Xu, A method to study interface diffusion of arsenic into a Nb–Ti microalloyed low carbon steel, *Int. J. Miner. Metall. Mater.*, 19(2012), No. 9, p. 821.

[6] Q.H. Han, Y.L. Kang, X.M. Zhao, L.F. Gao, and X.S. Qiu, High-temperature properties and microstructure of Mo microalloyed ultra-high-strength steel, *Int. J. Miner. Metall. Mater.*, 18(2011), No. 4, p. 407.

[7] C.Y. Chen, H.W. Yen, F.H. Kao, W.C. Li, C.Y. Huang, J.R. Yang, and S.H. Wang, Precipitation hardening of high-strength low-alloy steels by nanometer-sized carbides, *Mater. Sci. Eng. A*, 499(2009), No. 1–2, p. 162.

[8] Y. Funakawa, T. Shiozaki, K. Tomita, T. Yamamoto, and E. Maeda, Development of high strength hot-rolled sheet steel consisting of ferrite and nanometer-sized carbides, *ISIJ Int.*, 44(2004), No. 11, p. 1945.

[9] H.W. Yen, P.Y. Chen, C.Y. Huang, and J.R. Yang, Interphase precipitation of nanometer-sized carbides in a titanium-molybdenum-bearing low-carbon steel, *Acta Mater.*, 59(2011), No. 16, p. 6264.

[10] S. Mukherjee, I.B. Timokhina, C. Zhu, S.P. Ringer, and P.D. Hodgson, Three-dimensional atom probe microscopy study of interphase precipitation and nanoclusters in thermomechanically treated titanium–molybdenum steels, *Acta Mater.*, 61(2013), No. 7, p. 2521.

[11] T. Gladman, Precipitation hardening in metals, *Mater. Sci. Technol.*, 15(1999), No. 1, p. 30.

[12] A.D. Batte and R.W.K. Honeycombe, Strengthening of ferrite by vanadium carbide precipitation, *Met. Sci.*, 7(1973), No. 1, p. 160.

[13] B. Liao and F.R. Xiao, Research on microstructure and strength-toughening mechanism of acicular ferrite pipeline steel, *Trans. Mater. Heat Treat.* 30(2009), No. 2, p. 57.

[14] L.Y. Lan, C.L. Qiu, D.W. Zhao, and X.H. Gao, Toughness of welding heat affected zone in high strength steel with low welding crack susceptibility, *Trans. China Weld. Inst.*, 33(2012), No. 1, p. 41.

[15] A. Phillips, H. Kaul, J. Burg, C. Killmore, J. Williams, P. Campbell, and W. Blejde, Effect of microstructure and texture on the edge formability of light gauge strip steel, *ISIJ Int.*, 51(2011), No. 5, p. 832.

[16] K. Kamibayashi, Y. Tanabe, Y. Takemoto, I. Shimizu, and T. Senuma, Influence of Ti and Nb on the strength-ductility-hole expansion ratio balance of hot-rolled low-carbon high-strength steel sheets, *ISIJ Int.*, 52(2012), No. 1, p. 151.

[17] K. Yamada, K. Sato, and H. Nakamichi, Analysis of nanometer-sized precipitates using advanced TEM, *JFE Tech. Rep.*, 5(2007), No. 9, p. 5.

[18] R. Okamoto, A. Borgenstam, and J. Agren, Interphase precipitation in niobium-microalloyed steels, *Acta Mater.*, 58(2010), No. 14, p. 4783.

[19] P. Li and J.A. Todd, Application of a new model to the interphase precipitation reaction in vanadium steels, *Metall. Trans. A*, 19(1988), No. 9, p. 2139.

[20] R.W.K. Honeycombe, Some aspects of micro-alloying, *Trans. Jpn. Inst. Met.*, 24(1983), No. 4, p. 177.

[21] R.A. Ricks and P.R. Howell, The formation of discrete precipitate dispersions on mobile interphase boundaries in iron-base alloys, *Acta Metall.*, 31(1983), No. 6, p. 853.

[22] R.W.K. Honeycombe and R.F. Mehl, Transformation from austenite in alloy steels, *Metall. Trans. A*, 7(1976), No. 7, p. 915.

[23] H.W. Yen, C.Y. Huang, and J.R. Yang, Characterization of interphase-precipitated nanometer-sized carbides in a Ti–Mo-bearing steel, *Scripta Mater.*, 61(2009), No. 6, p. 616.